WILEY | Hindawi

Research Article

Crystallization Behavior of Rapid-Compression-Induced Mesomorphic Isotactic Polypropylene during Uniaxial Stretching at Different Temperatures

Mingkun Xu, Jiaxiang Lin, Xiaolin Zhang, Zhenyin Li, Chuntai Liu, Changyu Shen, and Chunguang Shao (iD)

National Engineering Research Center for Advanced Polymer Processing Technology,
The Key Laboratory of Material Processing and Mold of Ministry of Education, Zhengzhou University, Zhengzhou 450002, China

Correspondence should be addressed to Chunguang Shao; shaochg@zzu.edu.cn

The uniform bulk mesomorphic iPP is prepared by rapid compression, and its structural evolution under stretching at different temperatures is studied by combining wide-angle X-ray diffraction and small-angle X-ray scattering. Results show that stretching can induce mesophase to crystallize into α-phase or promote this phase transformation synergistically with temperature, which depends on the selection of stretching temperature. When the temperature is lower than the glass transition temperature of rigid amorphous fraction (RAF), stress could make RAF devitrify firstly and then induce meso-α phase transition during the strain-softening process. As the temperature increases, the high temperature could induce meso-α phase transition to occur before the strain softening, while stretching could promote this transition. When the temperature is higher than a critical value around 100°C, the mesophase can be transformed into α-phase completely during stretching. SAXS results show that all the transformed α-crystal exhibits nodular morphology, and they are ductile with greatly enhanced deformability. Based on the results, a reasonable mechanism of meso-α transformation in the stretching process is proposed, explaining the phase transition that goes through several different steps.

1. Introduction

Isotactic polypropylene (iPP) is applied widely in various industries because of its excellent properties such as wonderful strength, modulus, and low cost. Properties of iPP are primarily affected by the crystalline phase including the crystal form and morphology [1–3]. iPP is a typical polymorphic polymer, consisting of α monoclinic crystal, β hexagonal crystal, γ orthorhombic crystal, and mesophase. Among them, the mesophase with ordering degree between the crystalline phase and amorphous phase exhibits nodular morphology rather than large spherulites [1, 4–11]. Due to this special morphology, mesomorphic iPP shows great deformability and easy processability at low temperatures and has attracted much attention. De Rosa et al. have shown that the formation of the mesophase is of great technological importance because it offers various options to tailor the

mechanical properties of polypropylene [2, 12, 13], and Mileva et al. reported that mesomorphic iPP can also afford the preparation of optically transparent films of iPP without employing optical clarifiers [14]. Generally speaking, rapid cooling is identified as a prerequisite for iPP mesophase formation, but the inferiority is that there is a temperature and even a cooling rate gradient distribution in the samples, so it is very difficult to control the cooling rate accurately or to obtain materials with uniform structures in bulk [5, 9, 10, 15–19]. Recently, we have proved that uniform bulk mesomorphic iPP can be prepared by rapid compression, and even its content ratio of mesophase and crystal is accurately controlled by changing the pressurization rate [20].

Mesomorphic iPP is unstable and difficult to be utilized directly. Therefore, in order to improve the performance of iPP, reprocessing of mesophase is more important compared to its formation. High-temperature treatment was widely

used to reprocess the mesophase [15–17, 21–27]. Zhao et al. reported that during the high temperature-induced meso-α phase transition, the chain segments in the mesophase will first partially melt to form a chain segment with correct helical chirality; then the partially correct helical chiral chains act as the α-crystal nucleus and further crystallize into α-crystals [8]. However, Marega et al. proposed that the meso-α phase transition is mainly achieved through molecular chain rearrangement rather than melting recrystallization [28]. Recently, Jiang et al. found that the RAF first undergoes devitrification and then acts as α nuclei to trigger the meso-α transformation at higher temperatures [7]. Though the mechanism of mesophase crystallization is still being debated, the consensus is that the crystallinity, the crystal grain size, and the generation of a thermally stable crystalline phase can be precisely modulated by controlling the crystallization temperature [6, 29]. For example, De Rosa et al. proved that by controlling the mesophase crystallization temperature and defect concentration, the properties of iPP can be well regulated, and a novel α-iPP material with high strength, modulus, and good toughness was prepared [2, 12, 13, 18, 30, 31], and many reports prove that the nodular morphology can be retained during the crystallization of the mesophase below 120°C [7, 8]. In summary, as a kind of representative and well-known metastable polymer materials, the study on the crystallization process in mesomorphic iPP could not only provide useful information to cognize the crystallization essence but also offer one novel method to tailor the crystalline structure and thus the properties for the product.

In addition to high-temperature treatment, uniaxial or biaxial stretching is commonly applied in iPP processing, during which stretching-induced crystallization (SIC) is an important issue attracting attention from both industry and academy for decades [32, 33]. Up to now, a large number of studies have been done on SIC in the mesophase of other polymer materials, such as polylactic acid, poly(dimethylsiloxane) and poly(ethylene terephthalate), and "mesophase nucleating," or "SIC precursor" was proposed based on experimental observations [34–40]. However, knowledge about strain-induced crystallization in mesomorphic iPP remains incomplete [41], and three possible reasons may exist. First, a large number of reports have focused on the stretching-induced destruction of iPP crystal into mesophase, which tends to ignore the relevant correlation between mesophase and crystal at the molecular level and the truth that mesophase can conversely transform into the crystal [29, 32, 42, 43]. Second, the mesomorphic iPP is generally prepared by rapidly cooling the static melt at a cooling rate of 100–1,000 K/s, limiting the preparation of large and uniform mesophase samples. Third, the formation of RAF is evidenced for both mesomorphic and crystalline iPP and RAF devitrification as the "frozen orders" play an important role to trigger the crystallization of mesophase; thus, the selection of stretching temperature has a great effect on the SIC behavior in mesomorphic iPP [7].

Aiming to investigate the crystallization behavior of mesomorphic iPP under stretching, uniform bulk mesophase samples were prepared through rapid compression by a homemade pressure device, and the relative structural evolution was investigated with in situ WAXD during the uniaxial stretching at different temperatures. Combined with the ex situ SAXS measurements, we observed that stretching can induce mesophase to crystallize into α-phase or improve meso-α conversion efficiency and shorten the conversion time. The role of RAF and the change of mesophase nodular structure in the SIC process were clarified. The synergistic effect of stretching and temperature on meso-α phase transition was also clarified. Furthermore, a plausible mechanism was proposed to illustrate the crystallization behavior of mesophase under stretching.

2. Results and Discussion

2.1. Structure and Thermal Behavior of the Mesophase. Before the deformation experiments, structures of the iPP samples prepared by rapid compression are characterized by WAXD as shown in Figure 1(a). According to the 1D-WAXD profiles, two broad scattering halos of mesomorphic iPP were observed at 2θ of 15.0 and 21.0°, which has been reported the first peak reflects the average distance between molecular chains and the second peak represents the repetition period within the 3_1 helices of molecular chains [14, 27]. The inserted 2D-WAXD pattern displays that the mesophase was not oriented, meaning the mold utilized in the rapid compression process was well sealed and the melt did not flow [44]. Figure 1(b) displays the heating curve of the mesophase from 20 to 200°C, where a small wide endothermic peak from 40 to 60°C and an exothermic peak near 100°C were observed. It is known that the exothermic peak was the crystallization peak that was regarded as a heating-induced meso-α phase transition, but for this small endothermic peak with the heat of fusion of about 4.4 J/cm³, there exist different interpretations. Ferrero et al. pointed out that the mesophase underwent melting and subsequent recrystallization during the endothermic process [23], but more and more recent reports indicate that the endothermic peak mainly originates from the devitrification of a rigid amorphous fraction ($T_{g(RAF)}$) [7, 44]. Combing these interpretations with the DSC results, we chose to conduct isothermal annealing and tensile experiments on iPP mesophase at five temperatures of 40, 50, 80, 100, and 120°C, respectively.

2.2. Mechanical Behavior of the Mesophase. Figure 2(a) shows the stress-strain curves of the mesophase when stretched at different temperatures with the stretching rate of 10 μm/s, and all the curves show similar features of elastic, yield, strain softening, and strain hardening zones. With the strain increase, in the elastic zone, the stress increases almost linearly, and after yielding, it enters the strain-softening zone and decreases continuously, while after entering the strain hardening zone, it starts to increase, and the samples do not break even if the strain reaches 8.50. In addition, it found that as the stretching temperature increases, the yield peak gradually becomes insignificant and the corresponding yield strength gradually decreases. At the same time, the
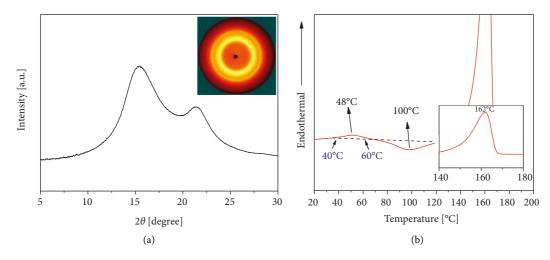
(a)

(b)

FIGURE 1: (a) WAXD 1D curve and 2D diagram of mesomorphic iPP and (b) DSC heating curve of the mesophase (the inset shows the melting peak region).
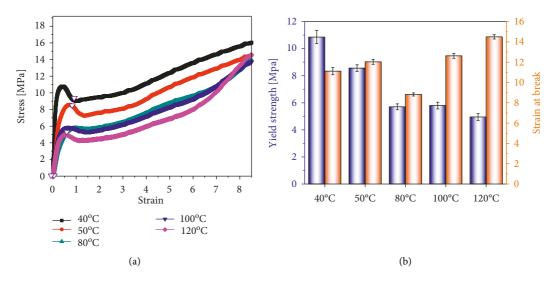

(a)

(b)

FIGURE 2: (a) The stress-strain curves of the mesophase under stretching at different temperatures (the purple triangles represent the initial crystallization point) and (b) yield strength and strain at break of the mesophase stretched at different temperatures.

corresponding strain at the yielding showed a trend of firstly increasing and subsequently decreasing. To further analyze the mechanical properties of the samples, the yield strength and strain at break are calculated and given in Figure 2(b). It displayed that as the tensile temperature increases, the yield strength decreases continuously from 10.8 MPa at 40°C to 4.9 MPa at 120°C, but the corresponding strain at break increases overall from 11.10 to 14.50, which means that all these samples are ductile material with greatly enhanced deformability.

2.3. In Situ WAXD Study on the Crystallization Behavior. The selected 2D WAXD patterns collected during the stretching of the mesophase samples are displayed in Figure 3. The meridian is defined in the parallel direction, while the equator is defined in the perpendicular (stretching) direction as indicated by the blue double-headed arrow. For the convenience to correlate the mechanical behavior and the 2D WAXD pattern, four zones are denoted. Uniform

diffraction rings are detected before stretching, and the scattering intensity begins to concentrate toward the equator and forms a crescent shape beyond the yield point, which means the orientation starts, and it becomes apparent in the subsequent softening or hardening zone. It shows that mesocrystal transformation takes place at all the selected temperatures, and the mesophase orientates before crystallizing under stretching at 40 or 50°C, but it crystallizes before orientating when stretched at high temperatures of 80, 100, or 120°C.

Figure 4 shows the 1D integrated WAXD curves of the 2D patterns under different stretching temperatures. It represents that the characteristic scattering halos of mesophase shift gradually, and the diffraction peaks of (110), (040), (130), and (111) for α-phase emerge step-by-step, corresponding to 2θ of 14.6, 16.7, 18.5, and 21.5°. It can be seen that when the mesophase sample is stretched at 40 or 50°C, the scattering intensity of α-phase emerges at a strain of about 0.96 and 0.76, respectively, but keeps relatively weak
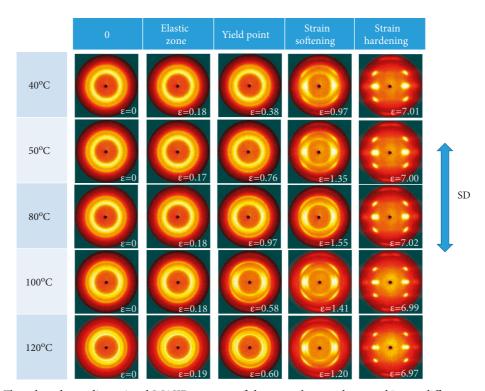
FIGURE 3: The selected two-dimensional WAXD patterns of the mesophase under stretching at different temperatures.

despite reaching a large strain of 8.00, indicating that a small amount of α-crystal was formed. When stretching at 80°C or higher, the scattering intensity of α-phase appears at the strain of about 0.57, while a continuous enhancement of the intensity was led to with higher strain, suggesting that a large amount of α-crystal was induced. According to the above results, the meso-α transition points are marked in the stress-strain curves in Figure 2(a).

To quantitatively analyze the change of the content for different phases, a representative fitting is performed on the WAXD profiles by analyzing a peak-fitting procedure as given in Figure 5(a), and the full spectrum is considered as a superposition of a number of reflections. During the fitting process, a total of 7 diffraction peaks need to be fitted, which consists of four crystal peaks of the α phase, corresponding to 2θ of 14.6° (110), 16.7° (040), 18.5° (130), and 21.5° (111); two characteristic peaks of iPP mesophase, corresponding to 2θ of 15.0° and 21.0°; and one amorphous peak, corresponding to 2θ of 17.0°; each diffraction peak is fitted using a Gaussian function. The specific crystallinity changes are summarized in Figures 5(b)–5(f), and the orientation degree of mesophase was also displayed. The degree of orientation of the stretched samples was calculated by formulas (3) and (4). It can be seen that as the deformation is performed, α-phase content increases at the cost of mesophase, indicating a direct transition from mesophase to α-phase. However, this transition behavior differs greatly at different temperatures. When the drawing temperature is 40 or 50°C (Figures 5(b) and 5(c)), it can be found that the critical orientation strain is 0.73 or 0.75, respectively, exceeding which the meso-α transition will take place. As stretching proceeds, the content of α-phase increases and reaches a

plateau at about the same strain of about 1.60, and the maximum value at 50°C is 16%, about two times that at 40°C (8%). The changing trend of crystallinity with strain is almost the same as that of the mesophase orientation, meaning the orientation plays an important role on the phase transition. When the temperature rises to 80°C (Figure 5(d)), meso-α phase transition takes place at a lower strain of 0.57 before the onset strain of mesophase orientation (0.77), and the crystallization and orientation changing trends are also highly similar, further suggesting the phase transition is mainly caused by the change of molecules orientation. When the temperate was set at 100 or 120°C, as shown in Figures 5(e) and 5(f), part of the mesophase has transformed to α-phase before stretching, and the α-phase content can reach the maximum value of about 34% at the strain of 1.60.

2.4. The Synergistic Effect of Stretching and Temperature on Meso-α Phase Transition. In order to clarify the synergistic effect of stretching and temperature on meso-α phase transition, the content changes of α-phase under stretching and isothermal annealing as a function of time are compared as given in Figure 6. No phase transition takes place during isothermal annealing at 40 or 50°C within 40 min; however, when the stretching is introduced, the phase transition emerges in a short time of about 240 s, which is in the strain-softening zone as Figure 2(a) shows. Clearly, in this case, stretching is the main inducement leading to the crystallization of mesophase, which can be considered a typical kind of SIC behavior. It has been known that the segments in mesophase are arranged in a low-order structure with the presence of helical reversals or wrong inclination of the
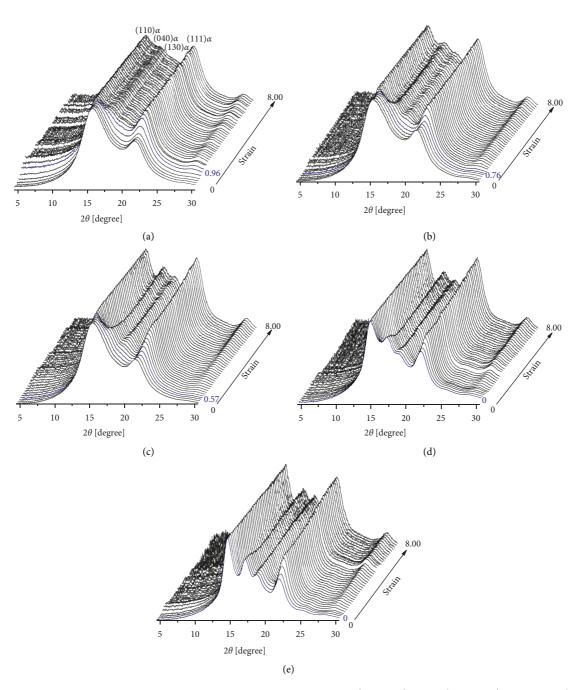
Figure 4: The selected 1D WAXD curves of the mesophase under stretching at (a) 40°C, (b) 50°C, (c) 80°C, (d) 100°C, and (e) 120°C (the blue curve relates to the strain where the mesophase starts to crystallize).

methyl groups of neighboring chains, and mesophase cannot transform into a crystal if the segments do not correct their helical chirality. Thus, it suggests that the strain-softening process should be corresponded to the helical chirality correction of mesophase and may also undergo the slips and/or the melting process of the order domains. Moreover, Androsch et al. proposed that the adjustment of mesophase helical chirality is completed by moving positions and rotating screws [45]. Thus, slips and/or the melting process of mesophase in the strain-softening process should be accompanied by the moving and/or rotating of the helical chirality, and subsequent helixes can grow and align,

inducing the formation of α-phase. Furthermore, when the mesophase is stretched at a sufficiently high temperature such as 100 and 120°C, which can greatly reduce the energy barrier for wrong chiral segments to adjust their helical chirality, temperature becomes the main inducement leading to the crystallization of mesophase, and the introduction of stretching can promote the meso-α transition in this condition.

Reports have shown that the mesomorphic iPP is mainly composed of three parts of mesophase, RAF, and the mobile amorphous fraction (MAF), where RAF is coupled at the boundary between the mesophase and the MAF [7]. It has
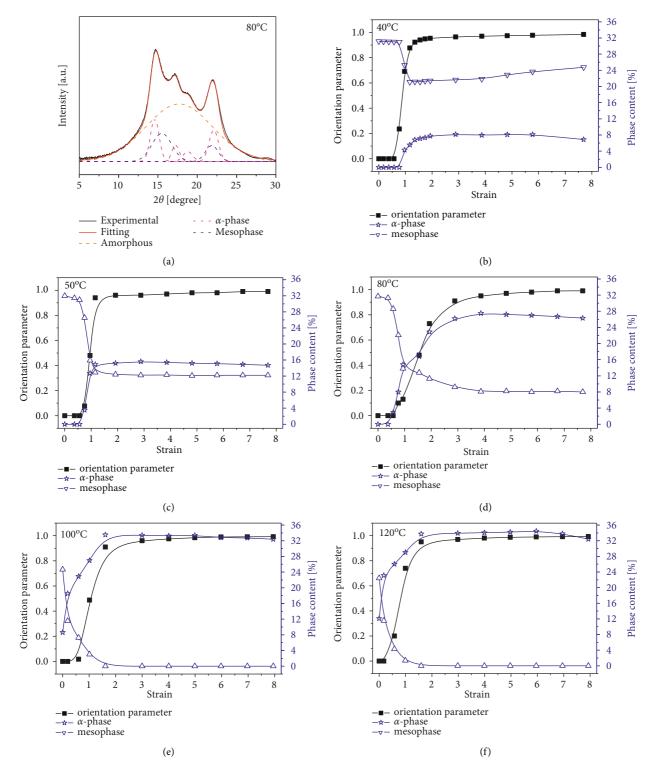
FIGURE 5: (a) The fitting curves of WAXD of amorphous, mesomorphic, and α phases and (b)–(f) the orientation parameter of mesophase and the content of α-phase as a function of strain at different temperatures.

also been proved that the RAF can not only impede the transport of new crystallizable segments to the growth face in the meso-crystal phase transition but also hinder the correction of wrong inclinations in the next crystal perfection process [44]. Therefore, it can be inferred that RAF should devitrify before SIC takes place. However, for the

α-phase obtained under stretching at 40°C, the temperature is not efficient to devitrify the RAF based on the DSC results; hence, a possible explanation is that the devitrification of RAF is caused by stress. Figure 6(f) shows that a work of 8.7 J/cm^3 is required to trigger SIC at 40°C, which is calculated with equation (1) based on the stress-strain curves.
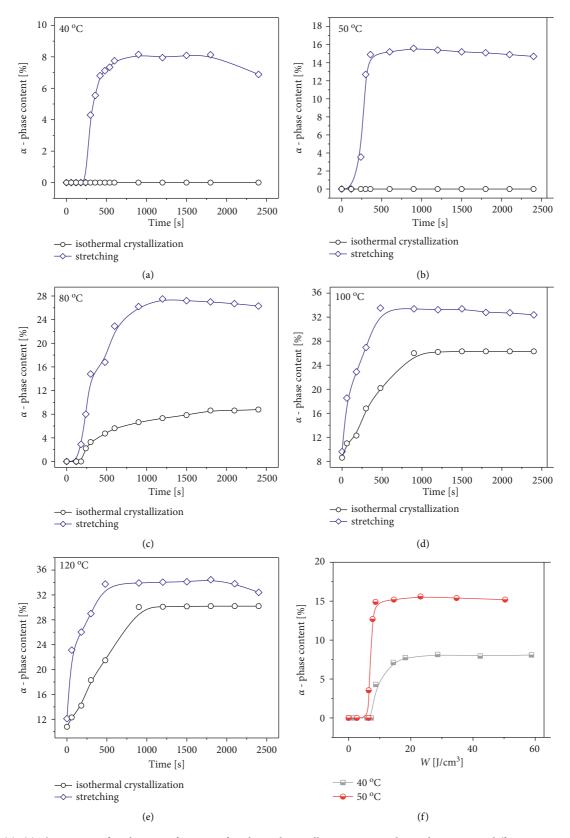
FIGURE 6: (a)–(e) The content of α-phase as a function of isothermal crystallization time and stretching time at different temperatures and (f) changes of the work as a function of α-phase content at 40 and 50°C.

When the temperature rises to 50°C that is slightly higher than the onset temperature of RAF devitrification but much lower than the cold crystallization temperature, partials of RAF can devitrify before stretching; thus, less work is needed to devitrify RAF, and it was calculated as 6.5 J/cm³, about 2.2 J/cm³ lower than that at 40°C. Interestingly, the reduction of the work almost equals the fusion heat absorbed by RAF devitrification (about 2.1 J/cm³ calculated from the DSC curves in Figure 1(b)) when heated from 40 to 50°C, indicating that the excess work done by the stress at 40°C mainly contributes to RAF devitrification. This result confirmed the prediction that stress can induce RAF devitrification at low temperatures.

Figure 7(a) summarizes and compares the maximum content of α-phase transformed from mesophase treated by stretching and isothermal crystallization as a function of temperature, and the conversion degree (defined as the ratio of the transformed content to the initial content) of mesophase is also taken into account. Clearly, the maximum content of α-phase obtained by stretching is always higher than that by isothermal crystallization, meaning that stretching can promote meso-α phase transition. For the samples treated by stretching, it was found that the conversion degree is small (about 32%) and the content of α-phase is as low as 8% when stretched at 40°C; with the temperature increase, the conversion degree increases and the crystallinity of α-crystal can reach an appreciable value of 28% after rising to 80°C; if the temperature increases to 100°C, the conversion degree reaches 100%, and the crystallinity of α-crystal gets to 34% and keeps constant despite higher temperatures. In general, the conversion degree of mesophase achieves a positive growth with temperature, and the mesophase can transform into α-crystal completely when stretching above a critical temperature around 100°C.

To further demonstrate the effect of stretching on meso-α phase transition, the value of half-time of crystallization ($t_{1/2}$) (estimated from Figure 6) at different stretching temperatures is summarized in Figure 7(b). Actually, the rate of meso-α transformation is controlled by α-crystal growth, while the growth kinetics of crystal is mainly controlled by the secondary nucleation mechanism in the chain. When the temperature is lower than 80°C, stretching is the main inducement leading to the phase transition, where the orientation and relaxation processes of molecular chains need to be accounted for [46]. The higher the temperature, the more obvious the molecular chain relaxation, which is detrimental to the crystal growth; thus, $t_{1/2}$ rises with the temperature increase below 80°C. When the temperature arrives at 100°C, chain diffusion becomes the main factor to promote the secondary nucleation of α-crystal and that diffusion rate rises with temperature, leading to the phase transition accelerating and $t_{1/2}$ decreasing [7, 8].

2.5. Evolution of Nodular Structures. Figure 8(a) shows the selective one-dimensional SAXS profiles of mesophase at a strain of 0, 0.75, 1.50, and 5.00. Note that the strain of 0.75 is in the strain-softening zone of all the samples. A weak scattering peak at $q_{max} = 0.65 \, nm^{-1}$ was observed at the strain of 0, where the corresponding long period is 9 nm, and it was recognized as the average diameter of the mesophase nodular domains [44]. Changes over the long period are calculated and shown in Figure 8(b). It can be found that after deformation, the long period raises sharply with the strain before it arrives at 0.75, and the higher the temperature is, the faster it increases. With the strain exceeding 0.75, the increasing rate of the long period gradually slows down. To explain this phenomenon, the mesophase superstructure should be concerned, whose basic unit is considered to be a stack composed of nodular domains embedded in the amorphous phase and connected by a large number of tie molecules [7, 47]. Under stretching, tensile loading first leads to deformation of the amorphous phase; then tie molecules transfer the stress to mesophase, which then contributes to deformation. Similarly, tie molecules also contribute to the devitrification of RAF and thus the destruction or transition of mesophase nodules, including fine-coarse slipping and internodules separation, which should be the main factor for the sharp increase of the long period before the strain of 0.75. With the temperature rising, the diffusion of molecular chains in the amorphous region can be promoted, and it can lead to further increase of the long period. Furthermore, during the deformation, the α-crystals transformed from mesophase should maintain the original nodular morphology and be connected by a large number of tie molecules. Therefore, all the samples after stretching should be ductile and flexible with high deformability.

Based on the obtained results and recent reports, a schematic for the structure change of mesomorphic iPP under stretching is given in Figure 9. The mesophase model is mainly composed of mesophase, RAF, and MAF, with their content of about 33%, 44%, and 23%, respectively. When stretching is performed at temperatures below $T_{g(RAF)}$, a small amount of RAF connected to the mesophase will be destroyed by the stress after the yield point; then it begins to transform to α-phase in the strain-softening zone through slips or the melting-recrystallization process, and simultaneously, the separation and fine-coarse slipping of mesophase nodular domains take place. Under large strain, the mesophase can be highly oriented and RAF completely devitrified; however, due to the low stretching temperature, molecular chains do not have enough diffusion mobility to adjust their helical chirality sufficiently; thus, only a small amount of α-crystal can be obtained. If the temperature reaches 80°C, the combined effect of high temperature and deformation could induce the meso-α transformation before the strain-softening zone, while the molecular chain has higher diffusion mobility so that the separation and fine-coarse slipping of the nodular domains are more significant, and more α-crystal can be transformed. Under large strain, the formed α-crystals become more stable and perfect, and they are highly oriented along the deformation direction. Additionally, all the transformed α-crystals seem to maintain the nodular morphology and be connected by a large number of tie molecules, which is beneficial for greatly enhancing the product's deformability.
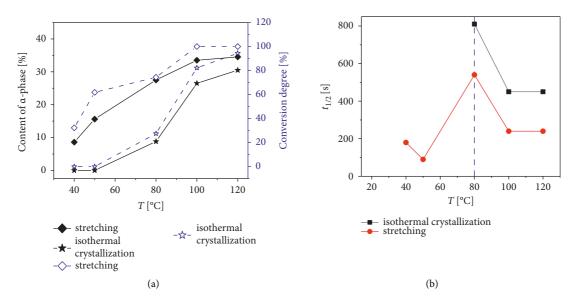
(a)

(b)

FIGURE 7: (a) Changes in the maximum content of α-phase and conversion degree of mesophase and (b) changes of $t_{1/2}$ during isothermal crystallization and stretching at different temperatures.
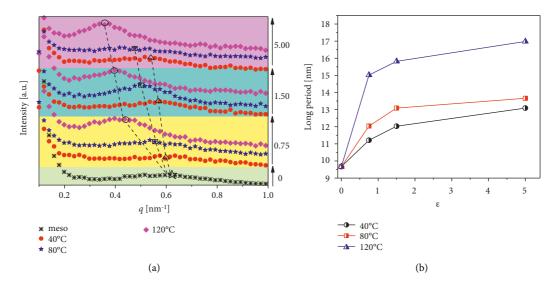

(a)

(b)

FIGURE 8: (a) One-dimensional SAXS curves at specific strains of the initial mesophase and that stretched at 40, 80, and 120°C and (b) variation of the long period as a function of specific strains stretched at 40, 80, and 120°C.
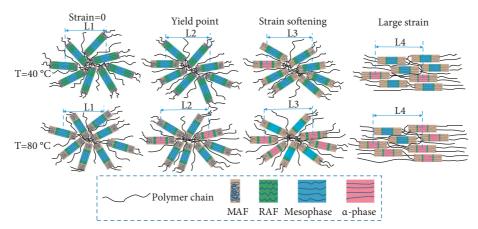

FIGURE 9: Schematic diagram of the structural change of mesomorphic iPP under stretching at different temperatures.

(a)   (b)
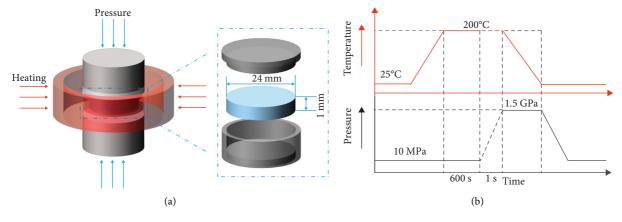
FIGURE 10: (a) Schematic of the high-pressure cell and (b) diagram of pressure and temperature for mesophase sample preparation.
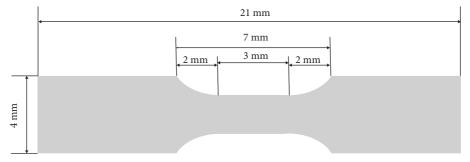

FIGURE 11: The schematic diagram of the initial tensile sample.

3. Conclusions

In this work, the uniform bulk mesomorphic iPP was obtained by rapid compression, and its crystallization behavior under stretching at different temperatures was studied. It is found that compared to the meso-α phase transition induced by isothermal crystallization, stretching not only can improve the meso-α conversion degree but also can shorten the transition time. At the temperature around $T_{g(\text{RAF})}$, stress can devitrify RAF in advance of the formation of the α-phase, and the chain orientation and relaxation play an important role in a subsequent meso-α phase transition, while the conversion degree is small. When the temperature increases, chain diffusion gradually becomes the main factor to induce meso-α phase transition, where stretching can promote the conversion degree, structural stability, and perfection. Moreover, there seems to be a critical temperature of around 100°C, above which the mesophase can transform into α-crystal completely within the scope of our experimental conditions. Finally, a reasonable mechanism of meso-α transformation under stretching was proposed, explaining the different steps that it undergoes. This work may offer a novel method to tailor the crystalline structure and thus the properties of iPP products.

4. Experimental Section

4.1. Materials and Sample Preparation. The iPP pellets (T30s) were purchased from Dushanzi Petrochemical Factory, China. The weight-average molecular weight and the polydispersity were 399 kgmol^{-1} and 4.6 respectively. The preparation process is shown in Figure 10. The circular sample (24 mm in diameter and 1 mm in thickness) was firstly prepared by compression molding; then it was treated by rapid pressurization through the homemade high-pressure equipment, and thereby, the initial mesophase sample was obtained. The pre-pressure of 10 MPa was applied to make the sample fully contact with the mold, and then it was heated to 200°C and maintained for 10 min to erase previous thermal history. Afterward, the melting sample at 200°C was rapidly pressurized to 1.5 GPa within 1 s and then cooled down to 40°C at an average cooling rate of about 10°C/min under 1.5 GPa; then the pressure was released; and the rapid compression (RC) sample was obtained. Finally, the RC sample was cut into a dumbbell shape, with 21.0 mm in total length, 3.0 mm in neck length, and 2.0 mm in neck width.

4.2. Tensile Experiments. All the samples were cut into a dumbbell shape, and their initial size was given in Figure 11. The tensile tests were performed using a tensile testing instrument (TST-350, Linkam, UK). The stretching rate employed was 10 μm/s; the heating rate employed was 10°C/min; and the stretching temperatures were 40, 50, 80, 100, and 120°C. For comparison, isothermal crystallization was performed at the same temperatures.

The deformation $(L - L_0)$ of the tensile samples was tested by a tensile testing instrument (TST-350, Linkam, UK) and then calculated according to $\varepsilon = ((L - L_0)/L) \times 100\%$, where the strain of the samples during the tensile

process can be obtained, and L is the actual length and L_0 the initial length of the tensile sample. According to the stress-strain ($\sigma - \varepsilon$) curve, the total work can be calculated as follows:

$$W = \int_0^\varepsilon \sigma \cdot d\varepsilon. \tag{1}$$

The total work (W) is the mechanical work per volume, which can eliminate the influence of sample size and shape when comparing different samples.

4.3. Characterizations

4.3.1. Wide-Angle X-Ray Diffraction (WAXD). In situ WAXD measurements were performed in conjunction with a tensile testing instrument (TST-350, Linkam, UK). The deformation rate adopted to collect in situ WAXS data was $10\,\mu$m/s. In situ WAXD measurements during the isothermal and stretching process were performed on an X-ray diffractometer (D8 discovery system, Bruker, Germany), with a wavelength of 0.154 nm and the distance between the sample and the detector of 85 mm. The VÅNTEC-500 two-dimensional area detector was used to record the two-dimensional patterns of WAXD. The exposure time of each pattern was 60 s. The VÅNTEC-500 two-dimensional area detector was used to record the two-dimensional patterns of WAXD. The patterns were acquired for the 2θ range between 5 and 35°. The exposure time of each pattern was 60 s. The FIT2D software package was used to analyze the 2D WAXD patterns, and the one-dimensional wide-angle X-ray diffraction curves were fitted according to the Gaussian function to obtain the crystallinities of different samples, and the phase content can be calculated by the following equations:

$$X_{\text{meso}} = \frac{A_{\text{meso}}}{\left(A_{\text{meso}} + A_\alpha + A_{\text{amorp}}\right)},$$
$$X_\alpha = \frac{A_\alpha}{\left(A_{\text{meso}} + A_\alpha + A_{\text{amorp}}\right)}, \tag{2}$$

where A_{meso}, A_α, and A_{amorp} are the fitted areas of mesophase, α-phase, and amorphous region, respectively. The orientation parameter (f) of the mesophase was generally expressed by

$$f = \frac{3\langle\cos^2\varnothing\rangle - 1}{2}, \tag{3}$$

where $\varnothing$ is the angle between the polymer chain and the stretching direction. $\langle\cos^2\varnothing\rangle$ can be obtained from the azimuth scattering intensity distribution by azimuthal integration of the 2D WAXD patterns and be calculated as follows:

$$\langle\cos^2\varnothing\rangle = \frac{\int_0^{(\pi/2)} I(\varnothing)\cos^2\varnothing \, \sin \, \varnothing d_\varnothing}{\int_0^{(\pi/2)} I(\varnothing)\sin \, \varnothing d_\varnothing}, \tag{4}$$

where $I(\varnothing)$ is the scattering intensity along the angle$\varnothing$. The orientation parameter attains a value of unity when all

the crystals are oriented with their interested axis parallel to the stretching direction, a value of -0.5 corresponds to a state that all the interested axes are perpendicular to the reference direction, while random orientation gives a value of 0. The orientation parameter was calculated from the WAXD scattering halo at 2θ of $15.0°$ of mesomorphic iPP.

4.3.2. Small-Angle X-Ray Scattering (SAXS). SAXS measurements were performed at room temperature using the Nanostar system of Bruker, with the wavelength of 0.154 nm and the distance from the sample to the detector of 1,087 mm. SAXS patterns were recorded with VÅNTEC-2000 two-dimensional area detector. The tested samples were prepared by stretching mesophase to the strain of 0, 0.75, 1.0, and 5.0 at different temperatures and then cooled down naturally, followed by removing the tension and relaxing to the final length. The middle region of the tensile samples was selected for SAXS measurement. The data acquisition time of each pattern was 600 s. The Bragg equation is used to calculate the long period of the samples:

$$L = 2\pi/q_{\text{max}}, \tag{5}$$

where L is the long period and q is the scattering vector.

4.3.3. Differential Scanning Calorimetry (DSC). The DSC calorimeter (TA DSC-Q2000) was employed in a nitrogen atmosphere to analyze the thermal behavior of the mesophase samples. Before the experiment, pure indium was used for calibration. The sample with a weight of about 4 mg was taken, and it was heated from 0 to 200°C at 10°C/min. The heat capacity was obtained by DSC three-step method with sapphire as the reference sample. The value of heat capacity was calculated with the following equation:

$$c_P^{\text{sp}} = c_P^{\text{cal}}\frac{m^{\text{cal}}\left(P_{\text{sp}} - P_0\right)}{m^{\text{sp}}\left(P_{\text{cal}} - P_0\right)}, \tag{6}$$

where m, c_p, and P are quality, heat capacity, and heat flow, respectively. The superscript sp and cal represent sample and reference sample, respectively. Through the DSC measurement, the heat flow of heating the sapphire (P_{cal}), sample (P_{sp}), and blank crucible (P_0) were measured.

Data Availability

The data that support the findings of this study are available from the corresponding author upon reasonable request.

Conflicts of Interest

The authors declare that they have no conflicts of interest.

Acknowledgments

References

[1] R. Krache, R. Benavente, J. M. Lopez-Majada, J. M. Perena, M. L. Cerrada, and E. Perez, "Competition between α, β, and γ polymorphs in a β-nucleated metallocenic isotactic polypropylene," *Macromolecules*, vol. 40, no. 19, pp. 6871–6878, 2007.

[2] C. De Rosa, F. Auriemma, R. Di Girolamo, and O. R. De Ballesteros, "Crystallization of the mesomorphic form and control of the molecular structure for tailoring the mechanical properties of isotactic polypropylene," *Journal of Polymer Science Part B: Polymer Physics*, vol. 52, no. 10, pp. 677–699, 2014.

[3] C. De Rosa and F. Auriemma, "Structural–mechanical phase diagram of isotactic polypropylene," *Journal of the American Chemical Society*, vol. 128, no. 34, pp. 11024-11025, 2006.

[4] K. Zapala, E. Piorkowska, A. Hiltner, and E. Baer, "High-pressure crystallization of isotactic polypropylene droplets," *Colloid & Polymer Science*, vol. 290, no. 16, pp. 1599–1607, 2012.

[5] K. Nishida, K. Okada, H. Asakawa et al., "In situ observations of the mesophase formation of isotactic polypropylene—a fast time-resolved X-ray diffraction study," *Polymer Journal*, vol. 44, no. 1, pp. 95–101, 2012.

[6] K. H. Nitta and K. Odaka, "Influence of structural organization on tensile properties in mesomorphic isotactic polypropylene," *Polymer*, vol. 50, no. 16, pp. 4080–4088, 2009.

[7] Q. H. Jiang, Y. Zhao, C. B. Zhang, J. Yang, Y. Z. Xu, and D. J. Wang, "In-situ investigation on the structural evolution of mesomorphic isotactic polypropylene in a continuous heating process," *Polymer*, vol. 105, pp. 133–143, 2016.

[8] J. C. Zhao, Z. G. Wang, Y. H. Niu, B. S. Hsiao, and S. Piccarolo, "Phase transitions in prequenched mesomorphic isotactic polypropylene during heating and annealing processes as revealed by simultaneous synchrotron SAXS and WAXD technique," *Journal of Physical Chemistry B*, vol. 116, no. 1, pp. 147–153, 2012.

[9] D. Mileva, R. Androsch, E. Zhuravlev, C. Schick, and B. Wunderlich, "Homogeneous nucleation and mesophase formation in glassy isotactic polypropylene," *Polymer*, vol. 53, no. 2, pp. 277–282, 2012.

[10] A. Mollova, R. Androsch, D. Mileva, M. Gahleitner, and S. S. Funari, "Crystallization of isotactic polypropylene containing beta-phase nucleating agent at rapid cooling," *European Polymer Journal*, vol. 49, no. 5, pp. 1057–1065, 2013.

[11] G. Colombe, S. Gree, O. Lhost, M. Dupire, M. Rosenthal, and D. A. Ivanov, "Correlation between mechanical properties and orientation of the crystalline and mesomorphic phases in isotactic polypropylene fibers," *Polymer*, vol. 52, no. 24, pp. 5630–5643, 2011.

[12] C. De Rosa, F. Auriemma, O. R. de Ballesteros, R. Di Girolamo, O. Tarallo, and N. G. Galotto, "Tailoring mechanical properties of isotactic polypropylene via crystallization of the mesophase and control of stereodefects concentration," *Macromolecular Chemistry and Physics*, vol. 214, no. 17, pp. 1951–1964, 2013.

[13] C. De Rosa, F. Auriemma, R. Di Girolamo et al., "Morphology and mechanical properties of the mesomorphic form of isotactic polypropylene in stereodefective polypropylene," *Macromolecules*, vol. 46, no. 13, pp. 5202–5214, 2013.

[14] D. Mileva, R. Androsch, and H. J. Radusch, "Effect of structure on light transmission in isotactic polypropylene and random propylene-1-butene copolymers," *Polymer Bulletin*, vol. 62, no. 4, pp. 561–571, 2009.

[15] D. Mileva, R. Androsch, E. Zhuravlev, C. Schick, and B. Wunderlich, "Formation and reorganization of the mesophase of isotactic polypropylene," *Molecular Crystals and Liquid Crystals*, vol. 556, no. 1, pp. 74–83, 2012.

[16] H. Asakawa, K. Nishida, J. Yamamoto, R. Inoue, and T. Kanaya, "Heating rate effects on the crystallization behavior of isotactic polypropylene from mesophase—a de-polarized light transmission study," *Polymer*, vol. 53, no. 13, pp. 2777–2782, 2012.

[17] D. Mileva, R. Androsch, E. Zhuravlev, C. Schick, and B. Wunderlich, "Isotropization, perfection and reorganization of the mesophase of isotactic polypropylene," *Thermochimica Acta*, vol. 522, no. 1-2, pp. 100–109, 2011.

[18] C. De Rosa, F. Auriemma, N. G. Galotto, and R. Di Girolamo, "Mesomorphic form of isotactic polypropylene in stereodefective polypropylene: solid mesophase or liquid-crystal like structure," *Polymer*, vol. 53, no. 12, pp. 2422–2428, 2012.

[19] G. Singh, S. Kaur, A. V. Kothari, D. G. Naik, P. B. Vyas, and V. K. Gupta, "Studies on the influence of molecular weight and isotacticity of polypropylene on the formation of mesomorphic phase," *Journal of Applied Polymer Science*, vol. 113, no. 5, pp. 3181–3186, 2009.

[20] J. J. Huang, X. B. Fu, C. G. Shao et al., "High-pressure induced formation of isotactic polypropylene mesophase: synergistic effect of pressure and pressurization rate," *Polymer Engineering & Science*, vol. 59, no. 3, pp. 439–446, 2019.

[21] D. S. Langhe, A. Hiltner, and E. Baer, "Transformation of isotactic polypropylene droplets from the mesophase into the α-phase," *Journal of Polymer Science Part B: Polymer Physics*, vol. 49, no. 23, pp. 1672–1682, 2011.

[22] V. Caldas, G. R. Brown, R. S. Nohr, J. G. Macdonald, and L. E. Raboin, "The structure of the mesomorphic phase of quenched isotactic polypropylene," *Polymer*, vol. 35, no. 5, pp. 899–907, 1994.

[23] A. Ferrero, E. Ferracini, A. Mazzavillani, and V. Malta, "A new X-ray study of the quenched isotactic polypropylene transition by annealing," *Journal of Macromolecular Science, Part B*, vol. 39, no. 1, pp. 109–129, 2000.

[24] X. Y. Li, J. J. Ding, Y. P. Liu, and X. Y. Tian, "A new model for mesomorphic-monoclinic phase transition of isotactic polypropylene," *Polymer*, vol. 108, pp. 242–250, 2017.

[25] X. Y. Li, Y. P. Liu, X. Y. Tian, and K. P. Cui, "Molecular mechanism leading to memory effect of mesomorphic isotactic polypropylene," *Journal of Polymer Science Part B: Polymer Physics*, vol. 54, no. 16, pp. 1573–1580, 2016.

[26] Q. H. Jiang, C. B. Zhang, J. Yang, Y. Zhao, Y. Z. Xu, and D. J. Wang, "Investigation on structural changes of isotactic polypropylene mesophase in the heating process by using two-dimensional infrared correlation spectroscopy," *Chinese Chemical Letters*, vol. 26, no. 2, pp. 197–199, 2015.

[27] X. Y. Li, F. M. Su, Y. X. Ji et al., "Influence of the memory effect of a mesomorphic isotactic polypropylene melt on crystallization behavior," *Soft Matter*, vol. 9, no. 35, p. 8579, 2013.

[28] C. Marega, V. Causin, and A. Marigo, "A SAXS–WAXD study on the mesomorphic-α transition of isotactic polypropylene," *Journal of Applied Polymer Science*, vol. 109, no. 1, pp. 32–37, 2008.

[29] S. A. Arvidson, S. A. Khan, and R. E. Gorga, "Mesomorphic-α-Monoclinic phase transition in isotactic polypropylene: a study of processing effects on structure and mechanical properties," *Macromolecules*, vol. 43, no. 6, pp. 2916–2924, 2010.

[30] C. De Rosa, F. Auriemma, O. R. De Ballesteros et al., "Stability and phase transformations of the mesomorphic form of

isotactic polypropylene in stereodefective polypropylene," *European Polymer Journal*, vol. 49, no. 11, pp. 3590–3600, 2013.

[31] C. De Rosa, F. Auriemma, O. Tarallo et al., "The "nodular" α form of isotactic polypropylene: stiff and strong polypropylene with high deformability," *Macromolecules*, vol. 50, no. 14, pp. 5434–5446, 2017.

[32] F. Auriemma, C. De Rosa, R. Di Girolamo et al., "Time-resolving study of stress-induced transformations of isotactic polypropylene through wide angle X-ray scattering measurements," *Polymers*, vol. 10, no. 2, p. 162, 2018.

[33] F. Zuo, J. K. Keum, X. M. Chen et al., "The role of interlamellar chain entanglement in deformation-induced structure changes during uniaxial stretching of isotactic polypropylene," *Polymer*, vol. 48, no. 23, pp. 6867–6880, 2007.

[34] J. Hu, L. L. Han, T. P. Zhang, Y. X. Duan, and J. M. Zhang, "Study on phase transformation behavior of strain-induced PLLA mesophase by polarized infrared spectroscopy," *Chinese Journal of Polymer Science*, vol. 37, no. 3, pp. 253–257, 2019.

[35] S. Baseri, M. Karimi, and M. Morshed, "Study of structural changes and mesomorphic transitions of oriented poly (ethylene therephthalate) fibers in supercritical CO_2," *European Polymer Journal*, vol. 48, no. 4, pp. 811–820, 2012.

[36] S. Baseri, M. Karimi, M. Morshed, and M. Youssefi, "Effect of drawing temperature on mesomorphic transitions of oriented poly(ethylene terephthalate) fibers exposed to supercritical CO_2," *Journal of Polymer Research*, vol. 18, no. 6, pp. 2033–2043, 2011.

[37] G. Stoclet, R. Seguela, J. M. Lefebvre, and C. Rochas, "New insights on the strain-induced mesophase of poly (d, l-lactide): *in situ* WAXS and DSC study of the thermo-mechanical stability," *Macromolecules*, vol. 43, no. 17, pp. 7228–7237, 2010.

[38] J. Y. Zhao, P. Z. Chen, Y. F. Lin et al., "Stretch-induced intermediate structures and crystallization of poly(-dimethylsiloxane): the effect of filler content," *Macromolecules*, vol. 53, no. 2, pp. 719–730, 2020.

[39] J. K. Keum and H. H. Song, "Thermal deformations of oriented noncrystalline poly (ethylene terephthalate) fibers in the presence of mesophase structure," *Polymer*, vol. 46, no. 3, pp. 939–945, 2005.

[40] R. H. Lv, S. F. Zou, B. Na, H. Y. Deng, and Z. W. Yu, "Influence of mesophase-crystal transition on thermal and mechanical properties of stretched poly (L-lactide)," *Polymer Engineering & Science*, vol. 53, no. 12, pp. 2568–2572, 2013.

[41] J. Qiu, Z. G. Wang, L. Yang, J. C. Zhao, Y. H. Niu, and B. S. Hsiao, "Deformation-induced highly oriented and stable mesomorphic phase in quenched isotactic polypropylene," *Polymer*, vol. 48, no. 23, pp. 6934–6947, 2007.

[42] Z. Ma, C. G. Shao, X. Wang et al., "Critical stress for drawing-induced α crystal–mesophase transition in isotactic polypropylene," *Polymer*, vol. 50, no. 12, pp. 2706–2715, 2009.

[43] X. W. Chen, F. Lv, F. M. Su et al., "Deformation mechanism of iPP under uniaxial stretching over a wide temperature range: an in-situ synchrotron radiation SAXS/WAXS study," *Polymer*, vol. 118, pp. 12–21, 2017.

[44] X. B. Fu, W. X. Jia, X. T. Li et al., "Phase transitions of the rapid compression induced mesomorphic isotactic polypropylene under high pressure annealing," *Journal of Polymer Science Part B: Physics*, vol. 57, no. 11, pp. 651–661, 2019.

[45] R. Androsch, "In situ atomic force microscopy of the mesomorphic–monoclinic phase transition in isotactic polypropylene," *Macromolecules*, vol. 41, no. 3, pp. 533–535, 2008.

[46] W. Luo, J. P. Wang, Y. Q. Guo, and W. B. Hu, "Role of stress relaxation in stress-induced polymer crystallization," *Polymer*, vol. 235, Article ID 124306, 2021.

[47] B. Wunderlich and J. Grebowicz, *Advances in Polymer Science*, Springer, Berlin, Germany, 1984.